Prospects of in-situ α-Al_2O_3 as an inoculant in Aluminium- a feasibility study

V.M.Sreekumar[1,a*], N. Hari Babu[1,b], D.G.Eskin[1,c]

[1]BCAST, Brunel University London, UB8 3PH, United Kingdom

[a] Email:Sreekumar.VadakkeMadam@brunel.ac.uk

[b]Email:Hari-Babu.Nadendla@brunel.ac.uk

[c]Email:Dmitry.Eskin@brunel.ac.uk

Abstract

In-situ α-Al_2O_3 was successfully synthesized and dispersed in Al alloy using B_2O_3 and ultrasonication aided liquid mixing technique. Microstructure analysis identified α-Al_2O_3 as the most common phase in the composite master alloy whereas AlB_{12} was frequently observed and AlB_2 was rarely found in the alloy. Grain refinement analysis of selected Al alloys registered a transition of columnar to equiaxial grains of α-Al with the inoculation of the master alloy and ultrasonication treatment. Similarly, an improvement in the mechanical properties of A357 alloy was observed with the combination of inoculation and ultrasonication treatment.

Key words: in-situ composites, α-Al_2O_3, grain refinement, ultrasonic cavitation

1. Introduction

Oxides are high melting point ceramic compounds having special physical and mechanical properties. Al_2O_3, SiO_2, alumina silicate, flyash are a few examples of oxides commonly used as reinforcements (fibers, whiskers, particles, etc.) in metal-ceramic composites in order to increase the strength and creep properties of the alloy [1]. A simpler and economical liquid metallurgy technique (impeller mixing or stir-casting) is widely used to disperse the oxides in liquid Al. Usually in all metal-ceramic composite systems, wettability is one of the important factors that defines the interfacial bonding and load transfer properties between metal and reinforcement [1-2]. While looking at the wettability properties of different ceramic materials, oxides are the worst performing because of the high contact angle (wetting angle) that forms with molten Al [1]. Hence, establishing wettability between oxides and molten Al is challenging, even more in the case of composite manufacturing through stir-casting

process. Lack of wetting often results in clustering and rejection of particles in the molten metal while mixing by an impeller [3]. Wettability properties of oxides with aluminium is generally improved by changing the composition of Al with the addition of elements like Mg, Cu, Ti etc, where Mg is found as the most successful wetting agent (surfactant) [1-4]. Mg has another role as the scavenger of oxygen entrapped inside the pores of the particles by nature or during mixing [3].

For the past decades, Al_2O_3, $MgAl_2O_4$, and MgO compounds were investigated as the interfacial reaction phases in oxide reinforced Al MMCs [5-9]. In effect, these interfacial products improve the wetting and prevent the degradation of reinforcement [1]. In recent times, research on the composites is essentially concentrated on the in-situ formation of these phases as reinforcements at high percentage (in-situ MMCs). Among the various processes established until now, the displacement reactions between the liquid metal and the ceramic oxides are found to gain interest, because of the thermodynamic feasibility of the reactions at the experimental conditions [10]. The materials such as SiO_2, CuO, TiO_2 etc. are recognized as the volatile ceramic oxides amenable for the in-situ generation of Al_2O_3, $MgAl_2O_4$, and MgO in Al alloy [5, 9, 11]. The Al_2O_3-$MgAl_2O_4$-MgO phase equilibria (reflective of volatile oxides dispersed in liquid Al) was studied by thermodynamic models and experimentally verified with different Mg composition of matrix alloy elsewhere [12]. The studies established that Al_2O_3 is stable at Mg content <0.19 wt%, whereas $MgAl_2O_4$ is stable between 0.007 and 10 wt% Mg and MgO is stable at >7 wt% Mg [12]. While volatile oxides enable the in-situ oxide particle formation in Al, the dispersion of volatile oxides (by impeller) is found difficult without any wetting agent. More often, a successful dispersion of the volatile oxides in Al is achieved by more Mg containing Al alloy. This means that the formation of Al_2O_3 as in-situ phase in molten Al becomes less feasible. As a matter of fact, in-situ Al_2O_3 dispersion in liquid Al by stir-casting technique is not reported, however studies are available in Al-oxide powder compacts and infiltration of pure aluminium in oxide preforms [13, 14].

Recently, grain refinement was reported in oxide- containing Al alloys. Atamanenko et al [15] looked at the grain refinement of pure Al possibly by ultrasonic cavitation-induced heterogeneous nucleation through the activation of externally added Al_2O_3 particles. Li et al [16] and Kim [17] demonstrated grain refinement of Al-Mg alloys using an intensive melt shearing technique and proposed a mechanism related to heterogeneous nucleation of Al on naturally occurring $MgAl_2O_4$ or MgO particles in Al alloys. Sreekumar et al observed an

appreciable reduction of grain size in Al-Mg-$MgAl_2O_4$ in-situ composite possibly by the presence of in-situ $MgAl_2O_4$ [5]. Further, Sreekumar et al systematically examined grain refining potency and efficiency of $MgAl_2O_4$ in Al alloys by a master alloy method [18]. Even though Al_2O_3 phase is present naturally (in-situ) in Al aplenty, no reports are available on the grain refinement of Al using in-situ Al_2O_3 particles as inoculants.

For the first time in authors knowledge, this paper reports on a technique for the synthesis and dispersion of in-situ α-Al_2O_3 in liquid Al. Being an important oxide phase presents in Al, grain refinement potential of α-Al_2O_3 in Al alloys is examined by a master alloy method. The composite is used as the master alloy for the grain refinement experiments in commercial and model Al alloys. Mechanical properties of one of the commercial Al alloys is examined after the inoculation technique.

2. Materials and methods

Commercially pure Al (CPAl, 0.08 wt% Si, 0.1 wt% Fe, remaining Al) and B_2O_3 were taken as starting materials. The initial particle size of B_2O_3 supplied from Sigma-Aldrich was in the range of 30-70 µm. B_2O_3 powder undergoes crystallographic changes at higher temperatures and subsequently melts at 440 ^oC to form a glassy structure. Hence, B_2O_3 particles immediately transform to viscous liquid inside the molten metal. Added to that, the density of B_2O_3 changes from 2.5g/cc to 1.8g/cc after the melting point, which is less than the density of liquid aluminium (2.3g/cc). Initially, the alloys were melted and treated in a boron nitride coated clay graphite crucible at a temperature between 700 ^oC and 900 ^oC. B_2O_3 particles were mixed using a mechanical impeller made from Ti alloy and coated with a high temperature ceramic glue to minimize impeller erosion during processing. The metal was ultrasonicated (water-cooled magnetostrictive system, Realtec, Russia, 17.5 kHz, 3.5 kW, 40 µm peak to peak amplitude, Nb sonotrode) to ensure the dispersion of particles and the completion of reaction. The Al_2O_3 content in the cast sample (referred to as master alloy (MA)) was approximated using reaction (1) shown later in the paper.

Grain refinement assessment was conducted on a commercial alloy (A357-7.4 wt% Si, 0.5 wt% Mg, 0.1 wt% Fe, 0.1 wt% Ti, remaining Al) and model alloys (CPAl and Al-1Si-0.5Mg alloys). The master alloy was added to 300g of molten alloy at 760 °C and cast at 750 °C in a steel mould (cooling rate ~2 °C/s) preheated to 250 °C before casting (Figure 1). In some experiments, the alloys were treated with ultrasound for 3 min at 740-750 °C before casting

(ultrasonic processing parameters were the same as shown above for the master alloy). In all the cases, cast samples were ground using SiC paper (400-2500 grid size) and polished using OPS. For identification of grain size, polished samples were anodised using 4% HBF_4 solution for approximately 1 min at 20 VDC and analysed in polarized light in an optical microscope (Zeiss Axioscope). Microstructure of the alloys were investigated using optical microscopy (Zeiss Axioscope) and phase identification in the master alloy was performed using X-Ray Diffraction (Bruker D8 Advance) and scanning electron microscopy (Zeiss Supra 35VP) coupled with Energy Dispersive Spectroscopy (EDAX).

Cooling curves of the selected compositions from liquid to solid transformation were measured with K-type thermocouples and recorded by means of dedicated software (NI-LABVIEW Data Logger) collecting 100 data per second. The steel mould used for grain refinement study was preheated to 350 °C and covered with ceramic wool in order to minimize the heat loss. The thermocouple was positioned from the top between the centre and the wall of the mould. The 300 g of A357 alloy was poured at a superheat of 100 °C above the liquidus of the alloy (620 ^{o}C).

The tensile tests of machined specimens (4 samples for each condition) were carried out in Instron 5569 with 50 kN load cell (ASTM E8). The sample dimensions of ASTM standard B557-cylindrical specimen with a gauge length of 25 mm-were cast in a permanent steel mould (1 kg melt charge). The casting conditions were kept similar to those of microstructural studies. Prior to testing, all test bars were heat treated. The samples were solutionized for 12 h at 540 °C, water quenched (warmed at 50 ^{o}C) and subsequently aged at 170 °C for 12 h. Elongation of the samples was recorded using an external extensometer (25-mm gauge length) and the yield stress was calculated by the offset method.

3. Experimental

3.1. Technique to produce an Al-Al_2O_3 master alloy

3.1.1. Mixing of B_2O_3 particles in CPAl

We started with testing a simple approach. B_2O_3 particles wrapped in Al foil was added to CPAl while impeller was running to form vortex. Glassy B_2O_3 was found to stick on the stirrer initially and floated to the top of the metal subsequently. The metal containing B_2O_3 was held at 900 ^{o}C for 30 min and cooled down to 700 ^{o}C. Later, the metal was mechanically

mixed using impeller at 700-720 ^{o}C for 5 min. The holding-mixing cycle was repeated 3-4 times until casting was performed. In another trial, molten CPAl was poured onto the molten B_2O_3 at 750 ^{o}C and mixed by ultrasonication for 5 min at 730-750 ^{o}C in order to disperse the liquid B_2O_3 directly. Similar to previous trial, holding-mixing was repeated 3-4 times until casting was performed. In both the cases, large lump of viscous B_2O_3 was visibly found separated on the top of the metal before casting. The metal was cut cross sectional to find the particles entrapped into the metal. The microstructure shows large B_2O_3 clusters in the metal (Figure 2 (a)) and close observation of the lump revealed the sign of reaction, where small clusters of product crystals were observed (shown by arrows in Figure 2 (b)). It was inferred that both methodologies were just good enough for introducing B_2O_3 in Al as some of the B_2O_3 was gone into the metal, but not sufficient to disperse B_2O_3 or reaction products.

3.1.2. Mixing of B_2O_3 in Al-0.4Mg alloy

In the third trial, B_2O_3 was mixed using impeller and ultrasonication in an Al-0.4 wt% Mg alloy. In order to achieve low surface tension and improve wettability with B_2O_3, 0.4 wt% Mg was added in CPAl initially. 5 wt% of B_2O_3 particles was stirred in molten Al-0.4 wt% Mg alloy at temperatures between 650 °C and 700 °C by an impeller and subsequently ultrasonicated for 5 min at 700-720 ^{o}C. The mixed melt was held at 900 °C for 30 mins to facilitate the reaction between oxide particles and liquid Al. Subsequently, the temperature was decreased to 700-720 ^{o}C and the melt was ultrasonicated for 5 min while impeller was running to ensure the dispersion of reaction product and complete reaction of B_2O_3. The cycles of holding and mixing processes were repeated 3-4 times and cast at 750 ^{o}C. The B_2O_3 was introduced much easier, most likely by the presence of Mg that initially stabilized the glassy liquid inside molten Al to facilitate the reaction and later on the dispersion of B_2O_3 and products in mixing-holding cycles.

This method of introduction, reaction and dispersion of oxides was chosen and the results are presented below.

4. Results and Discussion

4.1. Reaction products

The reaction between B_2O_3 and Al can be represented as [19]:

$$2Al + B_2O_3 = \alpha\text{-}Al_2O_3 + 2B \quad (1)$$

ΔG^{o}_{298}=-416.9 kJ/mol (2)

ΔH^{o}_{298}=-402.7 kJ/mol (3)

It is clear that Gibbs free energy of formation of Al_2O_3 from B_2O_3 is negative and an exothermic reaction occurs at the interface between molten Al and B_2O_3. From X-ray diffraction of the master alloy, only α- Al_2O_3 phase and Al were detected (Figure 3). Since no B_2O_3 was noticed, the reaction (1) was assumed to be completed forming Al_2O_3 and atomic boron (B). According to reaction 1, 5wt% of B_2O_3 forms 7.6wt% (5.9 vol%) Al_2O_3 and 1.5wt% B. Figure 4 shows the optical micrographs of Al-1.5B-7.6 Al_2O_3 master alloy where a few µm sized particles- likely to be Al_2O_3- were found to be distributed in the alloy (represented by arrows). SEM-EDS analysis (Figure 5) confirmed the compound as Al_2O_3 by the presence of oxygen and aluminium on the particles (shown by arrows). Also large blocky shaped particles of 40-50 µm in size were frequently observed in microstructure (Figure 4). Usually, matrix Al reacts with boron and forms AlB_2 or AB_{12} depending on the temperature of processing. The compounds can be differentiated in backscattered SEM, where dark particles relate to AlB_{12}, while light gray ones usually AlB_2. First, large blocky shaped particles were confirmed as boron bearing compound and further AlB_{12} in backscattered SEM (Figure 6). The EDS analysis detected Al, Mg and B on the compound with atomic percentage 7.14, 4.22 and 88.64 and the formation of AlB_{12} compound was confirmed. Interestingly, the result shows a substitutional diffusion of Mg in AlB_{12} likely during the reaction with Al-0.4Mg alloy and B_2O_3. A mutual diffusion of Al or Mg in AlB_2, AlB_{12}, MgB_2, MgB_{12} as well as the formation of several transition and stable compounds at different conditions were reported in previous studies [20]. In addition to the large particles, fine AlB_{12} particles of 3-4 µm in size were also found in the alloy. Microstructure (Figure 6) also shows the agglomeration of Al_2O_3 particle yet to be separated apart (shown by arrows). The chains of Al_2O_3 particles are formed at the unstable interface between liquid B_2O_3 and molten Al. Figure 7 shows particle size distribution of Al_2O_3 in the master alloy measured by *Imagej* software. It is very clear that around 60% of the particles tested (total 2000 no) lie between 1 and 3 µm and 90% of the particles has a size between 1 and 9 µm. Average particle size of Al_2O_3 was calculated to be 1.8 µm from the analysis. Similarly, the area/volume fraction of the particles in the microstructure was calculated to be 27%, which is considerably higher than the calculated volume fraction from reaction 1, i.e., 5.9%. It is known that for a given mass fraction, area fraction increases with increase in number of particles because of the increase in the total surface area of particles.

4.2. Mechanism of in-situ Al_2O_3 formation

During the introduction of liquid B_2O_3 into the molten Al-Mg alloy, low surface tension (aided by Mg) accompanied by downward force created by vortex provide the conditions for good and stable mixing. This is enough for B_2O_3 to establish reactive wetting with Al. The impeller mixing and ultrasonication result in the disintegration of liquid B_2O_3 releasing more surface area for the reaction. The influence of ultrasonication on the dispersion of ultrafine particles in molten metal was widely studied [21-23]. Also the formation, growth and implosion of cavitation bubbles during the alternate acoustic pressure wave cycles were observed in detail. Bubble implosion is a violent process producing pressure pulses (~1-5 GPa), temperature spikes (>4000 ^oC) and high velocity jets (100 m/s) in the liquid [21]. According to well-developed views, the cavitation threshold pressure is governed by the presence of cavitation nuclei such as vapor and gas bubbles, solid gas-absorbing suspensions and hydrophobic inclusions (oxides) [21]. It was experimentally demonstrated that the cavitation threshold pressure reduced from 800 to 550 kPa with the increase of alumina concentration in an aluminium melt from 0.005 to 0.1 wt% [21]. Further, the pressure sources the disintegration of intermetallics or particle agglomerates when present in the cavitation zone, depending on the threshold intensity required for the disintegration according to the equation [24]

$$I = 2W_l \left(\frac{\sigma_{stp}}{D\omega\rho_l}\right)^2 \qquad (4)$$

where, W is the ultrasonic power, ω is oscillation frequency, σ_{stp} is the tensile strength of particle or agglomerate, ρ is the density of the liquid, D is the diameter of particle or agglomerate. Normally the tensile strength of agglomerate is many order lower than the monolithic particle so is easy to disintegrate with a low stress. For example, Al_2O_3 monolithic particle has a tensile strength of ~500 MPa, whereas micron-sized Al_2O_3 agglomerates have a strength of ~75 MPa [25]. In the present experimental conditions reaction products are loosely held with the liquid B_2O_3 by surface tension and cavitation pressure must be able to disintegrate the liquid to smaller droplets and de-agglomerate the product clusters at a low pressure. However, surface area minimization can result in the coalescence of tiny droplets to form larger ones in a later stage. Since there is minimum crystallographic bonding exists within liquid B_2O_3, the reaction (1) should be fast with Al in all the cases. As a result, first layer of compound forms releasing boron to the metal. In the next stage, B reacts with Al and Mg at the interface to form transition compound. As the reaction proceeds, Mg content at the

interface decreases so that Al_2O_3 becomes more favorable. Both reactions are continued simultaneously to form Al_2O_3 and Al-Mg-B compounds in the final microstructure. A reduction in Mg concentration of the alloy due to its diffusion in AlB_2 compound was identified in AlB_2 reinforced Al MMCs [20]. Once the Mg concentration in the alloy is reduced to less than Al_2O_3-$MgAl_2O_4$ phase equilibrium composition (0.19wt%), the initially formed Mg bearing oxide such as $MgAl_2O_4$ may also transform to Al_2O_3 freeing Mg back into the alloy. This reaction mechanism reveals the possibility of Al_2O_3 formation in Al alloy at Mg content higher than the Mg required for Al_2O_3-$MgAl_2O_4$ phase equilibrium (0.19wt%).

The bi-modal distribution of AlB_{12} particles is need to be discussed further in view of the formation of crystals. It is very clear that there is appreciable difference in the size between small and large particles. During the mixing and dispersion process, liquid B_2O_3 is likely to be dispersed into small droplets and tiny AlB_{12} crystals are formed during the reaction. Similarly, bigger AlB_{12} crystals are formed on large droplets because the crystal growth depends on the boron concentration at the interface. Interestingly, close observations of some of the large crystals pointed towards the possibility of mechanical disintegration of large crystals into tiny ones. It was seen from the microstructures that large AlB_{12} crystals have polygonal shapes with smooth edges (face) and sharp corners. However, polygonals with irregular edges (faces) were also observed in the microstructures. This was further explained from the SEM (Figure 8) where the large particle having irregular face (indicated with straight line) and tiny crystals were found on the vicinity of the crystal face. These tiny crystals are most likely the debris that separated from the parent crystal during the disintegration process. Some of the features like sharp cut on one of the corners (arrow 1), a tiny crystal that was about to break out from the parent crystal (arrow 4) are most likely the signatures of mechanical disintegration. Morphologies of some of the small crystals (arrow 2and 3) have close resemblance with the cut off corner of the large crystal. Mechanical disintegration can be possible by the implosion of cavitation bubbles, which was previously reported for Al_3Ti intermetallic in Al [26].

AlB_{12} is stable at a temperature >975^0C or at boron concentration >44.5wt% according to the Al-B phase diagram [27]. Maximum solubility of boron in liquid Al between 660 and 975 ^{o}C is 0.022-0.35 wt%. So most of the boron released during the reaction stays at the interface and forms AlB_{12} compound when the local concentration reaches >44.5 wt% or the local temperature reaches 975 ^{o}C due to the exothermic nature of the reaction. As can be

understood from the experimental conditions such as temperature (700-900 ^{o}C) and boron concentration (0-1.5wt% max) that AlB_{12} cannot be stable once formed at the interface. Hence, at holding-mixing cycles, a thermodynamic driving force exists to transform the AlB_{12} to AlB_2. While the kinetics of transformation is sluggish for large particles, it may be quicker for tiny ones and grey particles found near the large crystal (arrow 5, Figure 8) are possibly the transformed AlB_2 particles. In short, Al_2O_3 is detected as the most occurring phase, while AlB_{12} crystals are frequently present and AlB_2 crystals are the rarest in the master alloy. This conclusion is very much important in finding the most probable inoculant in the master alloy for the grain refinement of Al alloys (forwarding section).

A few reports on the reaction between B_2O_3 and Al (solid/liquid) are available in literature. Birol [28] detected AlB_2 and Al_2O_3 in B_2O_3-pure Al powder mix at temperature, 875 ^{o}C, whereas AlB_{10} and Al-B-O compound started forming at a temperature, 1000 ^{o}C. Ficici et al [29] prepared Al-AlB_2 in-situ composites by the reaction between molten aluminium and B_2O_3 glass at 1400 ^{o}C. Several Al-B-O compounds were detected on the glass layer that was already floated at the top of the molten metal during the reaction. It can be inferred from the current and previous investigations that reaction between Al and B_2O_3 is complex in nature and interestingly, different phases are formed with respect to the experimental conditions employed.

4.3. Inoculation by an alumina-containing master alloys in Al alloys

Grain refinement potential of the master alloy (an addition level of 1 wt%) was explored in different model Al alloys such as CPAl, Al-1Si-0.5Mg and commercially important Al-7Si-0.5Mg-0.1Ti (A357) alloy. Also the influence of ultrasonication in the grain refinement was examined. Figure 9 shows the macro-etched cast billets of CPAl where large columnar grains were found in the as-cast samples (Fig 9 a and b). Columnar grains were still present in the master alloy added samples (Fig 9 c) whereas Columnar to Equiaxed Transition (CET) was observed in the samples ultrasonicated after the master alloy addition (Fig 9 d). The CET was further substantiated from the anodized CPAl micrographs (Figure 10) where large columnar grains (Fig 10 a) were found to transform into equiaxed and smaller grains with the addition of the master alloy and ultrasonication treatment (Fig 10 b). In Al-1Si-0.5Mg alloy, the large equiaxed grains with 600±23 μm in size were present in the reference sample (Figure 11).

After master alloy addition, the grain size was reduced to 400 ±12 µm and the ultrasonication helped in reducing the size to 240 ±12 µm (Figure 12). The Figures 13, 14 and 15 show the microstructures of A357 alloy inoculated with master alloy. It is very clear that 1wt% of the master alloy reduced the grain size of A357 from 900±30 µm (Fig 13 a) to 400 ±19 µm (Fig 14 a). With the application of ultrasonication, the grain size was drastically reduced to 190 ±10 µm in the master alloy added alloy (Fig 14 b). In order to understand the significance of minimal addition of the master alloy in comparison with the commercially important grain refiner Al-5Ti-1B, the addition was reduced to 0.1wt% (Figure 15). The grain size was reduced from 900 ±30 µm to 500 ±20 µm with the master alloy addition (Fig 15 a) and further reduction to 210 ±15 µm with the application of ultrasonication (Fig 15 b). It is very clear from the results that the master alloy is able to reduce the grain size of the alloy and the ultrasonication aids the refinement further.

Figure 16 presents the cooling curves of A357 alloy inoculated with 1 wt% of the master alloy. The alloys were cast in the same metallic mould (Figure 1) to measure the undercooling and the nucleation temperature of the primary Al grains and understand the heterogeneous nucleation mechanism of oxide inoculant. From the thermal analysis (Fig 16), the nucleation temperature (T_n) of primary Al crystals is identified from the first derivative of temperature (dT/dt - t) curve, where the slope of the T-t curve starts to deviate [30]. Other two temperatures are (a) T_{min}, unsteady state growth temperature or the onset of recalescence, where the latent heat liberated during nucleation surpasses the heat extracted from the sample and (b) T_g, the end of recalescence or the onset of steady state growth of primary α-Al dendrites. Consequently, the undercooling is approximated as $\Delta T = (T_g - T_{min})$ as in the case of the primary α-Al nucleation [30]. From Figure 16 (a), the Al primary phase started nucleating at 620 ^oC and ended at 618.5 ^oC in the reference alloy (the alloy without master alloy addition). The maximum nucleation undercooling from the recalescence was calculated to be 1.5 ^oC. In the presence of the master alloy in A357 alloy, nucleation of Al was found to start slightly above 620 ^oC and no recalescence was noticed in the cooling curve (Fig 16 b). The sharp peak found in the differential curve (Fig 16 a) further confirmed the presence of recalescence in A357 Alloys which was absent in the inoculated alloy (Fig16 b). The absence of recalescence is not uncommon in inoculated Al alloys at moderate cooling rates, 2 °C/s [31, 32]. This happens due to the increased number of heterogeneous nucleation events aided by numerous nucleant particles present in the alloy. The results of thermal analysis testify that master alloy contains potent nucleants for heterogeneous nucleation of α-Al. Note that

the limitations of data acquisition and thermocouple sensitivity can sometimes neglect a small change in the temperature.

Nucleation potency and efficiency of substrates are the important parameters to describe grain refinement of tested alloys; other parameters like cooling rate and composition are kept constant. The potency of a solid substrate in a liquid metal can be defined as the degree of lattice matching across the interface between the substrate and the solid phase to be nucleated. The lattice misfit f can be used as a quantitative measure of the potency for heterogeneous nucleation, and is defined as f = (dS – dN)/dS, where dS and dN are the atomic spacing along a close packed direction on a close packed plane of the solid and the nucleating substrate, respectively [33]. The calculated lattice misfit with solid Al at 660 °C is 3.38% for γ - Al_2O_3, –0.48% for α- Al_2O_3, indicating that these oxides are highly potent for nucleation of α-Al in consideration of the corresponding lattice misfit being –4.22% for TiB_2 [33]. Lattice misfit for AlB_2 (-5.1%) is quite similar to that of TiB_2, and AlB_{12} displays huge misfit with α-Al (115%) [34, 35]. This suggest that AlB_2 is potent nucleant but AlB_{12} not. Nucleation efficiency refers to the effectiveness of a given type of inoculant with specific physical characteristics and solidification conditions, such as number density, size distribution and cooling rate. For example, TiB_2 particle population in an Al-5 wt% Ti-1 wt% B master alloy was estimated to be 10^8 particles/cm^3 with average particle size of 1 μm [35]. Similarly, for the Al_2O_3 particles with average particle size 2 μm, the number density was approximated to 10^{11} particles/cm^3. According to the athermal heterogeneous nucleation theory, the nucleation and growth of the solid phase are not only related to the geometry of the nucleant particles, but also are determined by the undercooling, ΔTg, by the equation

$$\Delta T_g = 4\,\Gamma_{sl}/D \qquad (5)$$

where Γ_{sl} is the Gibbs–Thomson coefficient between the stable embryo of the solid phase and the liquid and D is the diameter of the critical nuclei after successful nucleation, which is equivalent to the diameter of particle. For an Al alloy, Γ_{sl} is about 9.12×10^{-8} ºCm [36]. In the present study, undercooling required for Al_2O_3 to nucleate aluminium was calculated to be in the range of 0.36-0.04 ºC for 1-9 μm and more 60% of the particles are >1.8 μm (ΔTg <0.2 ºC). In the present study, Al_2O_3 is qualified to be a possible nucleant for the grain refinement of α-Al.

AlB_2 is successfully used as an efficient inoculant for high Si containing Al alloys more than 4wt% Si [37]. Further, good grain refinement was demonstrated in Al-7Si alloy with the

addition of Al-B master alloy containing AlB_2 and AlB_{12} compounds [35]. All of the studies speculated a possibility of transformation of AlB_{12} to AlB_2 in the inoculation condition, but was not proven experimentally. According to the eutectic theory by Mohanty and Gruzelski, Al-B constitutes a eutectic at 0.022wt%B and 659.7 ^oC [38]. A lower addition of boron (<0.022wt%) results in the dissolution of AlB_2 and no nucleant will be available for heterogeneous nucleation, which holds true for low Si containing Al alloys (liquidus is near 659 ^oC. However, new AlB_2 precipitates in the alloy may act as nucleants in the Al-Si alloys containing more than 4wt% Si (liquidus is <659 ^oC). The dissolution-precipitation mechanism explained for AlB_2 doesn't hold true for AlB_{12} as the compound remains undissolved at longer period of time, which is substantiated in the present study. AlB_2 seems to be the rarest compound in the present study, which negates the possibility of it being an active nucleant for grain refinement. 1wt% of master alloy is equivalent to 0.015wt% Boron in the master alloy, which is less than the eutectic point of Al-B. It is confirmed by many investigators that grain refinement is insignificant in Al-7Si alloy at boron concentration less than 0.022wt% [35, 39, 40]. But current study explicitly showed that the master alloy is capable of reducing the grain size of Al-7Si alloy even at a boron concentration of 0.0015wt% (0.1wt% MA) (Figure 15). This underlines the fact that the influence of Al_2O_3 particles in the enhancement of grain refinement is substantial.

The influence of ultrasonication close to the liquidus temperature on the grain refinement of alloys was studied extensively [21]. A systematic study by Wang et al [41] in a non-inoculated alloy made clear that ultrasonication in complete liquid state had negligible effect on grain refinement, which is substantiated in recent studies by the authors (Fig 9 b and 13). It is important to note that ultrasonication gives additional grain refinement benefit when applied to the liquid metal containing inoculant particles. Manual stirring or mechanical stirring found to fail in distributing fine particles in liquid metal. Cavitation and associated acoustic streaming seem to be contributing to the distribution of inoculant particles within the metal ensuring more particles for the nucleation event. Recent work showed that ultrasonication is capable of dispersing in-situ $MgAl_2O_4$ particulates in liquid metal [5, 18]. It is clear from the microstructure analysis that the master alloy obtained in the current work contains homogeneously distributed Al_2O_3 (see Figure 4). During the addition of master alloy in molten Al, Al_2O_3 immediately comes in contact with the dissolved hydrogen. It was experimentally proven that alumina particles are active absorbent of hydrogen and stabilize the absorbed hydrogen on the surface of the particles. This may eventually prevent the

potential crystallographic planes to come in contact with Al for nucleation. Further, fine particles show a tendency to agglomerate due to the Vander Waals force, which in turn reduce the number density of the particles. Altogether, the nucleation potency and efficiency are negatively affected by both phenomena. During the ultrasonication treatment with an intensity higher than the cavitation threshold, cavitation bubbles are nucleated and grown on the particle surface. High energy pulsation and jet created during the bubble implosion disintegrate the particle agglomerates and strip off the gaseous layer, given that the nucleating surfaces are again accessible to the molten metal. This explanation is illustrated by the microstructures in Figure 17, where a large cluster of particles is observed in the non-ultrasonicated A357 alloy, while clusters are smaller after ultrasonication. Interestingly, clustered particles are found inside α-Al in both the cases. Columnar to Equiaxial Transition observed in CPAl and additional grain size reduction in other studied alloys signify the improvement in the potency and efficiency of Al_2O_3 particles after ultrasonication.

4.4. Mechanical properties

It is essential to testify the performance of a grain refiner in terms of the mechanical performance of the inoculated alloys. Figure 18 shows the tensile testing performance of aged A357 alloy inoculated with 1wt% of the master alloy. The stress-strain graphs of different alloys are denoted as 1, 2, 3 and 4. The yield strength, UTS and Elongation of the reference alloy (Fig 18-1) was found to increase after the ultrasonication treatment (Fig 18-2). The alloy inoculated with the master alloy showed an improvement in yield strength and UTS, but an appreciable reduction in elongation-most likely due to the particle agglomeration and associated defects-was noticed (Fig 18-3). The ultrasonication seemed to help in the improvement of elongation and UTS of inoculated alloy (Fig 18-4). However, no difference in the yield strength was noticed in both the inoculated alloys.

5. Conclusion

In-situ α-Al_2O_3 dispersed Al composite master alloy was prepared using B_2O_3 and ultrasonication aided liquid metallurgy route. α-Al_2O_3, AlB_{12} and AlB_2 compounds were identified in the master alloy, where α-Al_2O_3 was most commonly observed in the microstructure. Detailed microstructure analysis identified Mg atom diffusion in AlB_{12} compound and a possible transformation of AlB_{12} to AlB_2. Al_2O_3 particles of size between 1 and 9 µm were largely found in the microstructure. The grain refinement potential of the master alloy was successfully tested in model and commercial Al alloys. With the

combination of master alloy addition and ultrasonication, CET transition was observed in CPAl and 75% reduction in the grain size was achieved in A357 alloy. A detailed analysis identified the role of α-Al_2O_3 as nucleating substrate for the refinement of α-Al in the alloys. The ultrasonication treatment distributes the Al_2O_3 particles that subsequently provides enhanced heterogeneous nucleation events during solidification, resulting in the grain refinement of both CP Al and A357 alloys. A357 alloys exhibited an improvement in strength and ductility after inoculation and ultrasonication treatment.

Acknowledgement

The authors wish to acknowledge financial support from the ExoMet Project, which is co-funded by the European Commission in the 7th Framework Programme (contract FP7-NMP3-LA-2012-280421), by the European Space Agency and by the individual partner organisations.

References

1. R. Asthana, *Solidification Processing of Reinforced Metals*, 1998, Trans Tech Publications Ltd, Switzerland

2. P.K. Rohatgi, R. Asthana and S. Das, Solidification, structures, and properties of cast metal-ceramic particle composites, *International metals reviews,* 1986, 31 (1), p 115-39

3. G. Ramani, R.M. Pillai, B.C. Pai and T.R. Ramamohan, Factors affecting the stability of non-wetting dispersoid suspensions in metallic melts, *Composites*, 1991, 22 (2), p 143-50

4. T. P. D. Rajan, R. M. Pillai and B. C. Pai, Reinforcement coatings and interfaces in aluminium metal matrix composites, *J. Mater. Sci.*, 1998, 30, p 3491 – 3503

5. V.M. Sreekumar, N. H. Babu, D.G. Eskin, Z. Fan, Structure–property analysis of in-situ Al–MgAl2O4 metal matrix composites synthesized using ultrasonic cavitation, *Mater. Sci. Eng. A*, 2015, 628, p 30-40.

6. Y. Le Petitcorps, J.M. Quenisset, G. Le Borgne, and M. Bathole, Segregation of magnesium in squeeze-cast aluminium matrix composites reinforced with alumina fibres , *Mater. Sci. Eng. A*, 1991, 135, p 37–40

7. Y. Kim, J. C. Lee, Processing and interfacial bonding strength of 2014 Al matrix composites reinforced with oxidized SiC particles, *Mater. Sci. Eng. A*, 2006, 420, p 8–12

8. M.O. Lai, L. Lu, and B.Y. Chung: Formation of Mg-Al-Ti/MgO composite via reduction of TiO2, *Comp. Struct*., 2002, 57, p 183–87

9. G. Chen, G.X. Sun, and Z.G. Zhu Study on reaction-processed Al-Cu-AlB2-BOB3B (p) composites, *Mater. Sci. Eng.A*, 1999, 265, p 197–201

10. V.M. Sreekumar, On the formation of magnesium aluminates spinels in-situ in molten aluminium–magnesium alloys mixed with silica particles, 2008, Ph.D. thesis, Indian Institute of Technology, Kharagpur

11. D. Horvitz and I. Gotman, Pressure-assisted SHS synthesis of MgAl2O4–TiAl in-situ composites with interpenetrating networks, *Acta Mater.* 2002, 50, p 1961-71

12. V.M. Sreekumar, K.R. Ravi, R.M. Pillai, B.C. Pai and M. Chakraborty, Thermodynamics and Kinetics of the Formation of Al2O3/ MgAl2O4/MgO in Al-Silica Metal Matrix Composite, *Metall. Mater. Trans.A.* 2008, 39, p 919-33

13. M. Hanabe and P.B. Aswath, Synthesis of in-situ reinforced Al composite from Al-Mg-Si-O precursors, *Acta Mater.* 1997, 45, p 4067–76

14. D. Horvitz, I. Gotman, E.Y. Gutmanas and N. Claussen, In situ processing of dense Al2O3–Ti aluminide interpenetrating phase composites, *J.Eur.Ceram.Soc.,* 2002, 22, p 947–54.

15. T.V. Atamanenko, D.G. Eskin, L. Zhang and L. Katgerman, Criteria of Grain Refinement Induced by Ultrasonic Melt Treatment of Aluminum Alloys Containing Zr and Ti, *Metall. Mater. Trans. A.*, 2010, 41, p 2056-66

16. H.T. Li , Y. Wang and Z. Fan, Mechanisms of enhanced heterogeneous nucleation during solidification in binary Al–Mg alloys, *Acta Mater.*, 2012, 60, p 1528–37

17. K.Kim, The Effect of Melt Conditioning on Segregation of Solute Elements and Nucleation of Aluminum Grains in a Twin Roll Cast Aluminum Alloy. *Metal. Mater. Trans.A*, 2014, 45(10), p 4538-48

18. V. M. Sreekumar., N. H. Babu, D.G.Eskin and Z.Fan, Development of New Oxide Based Master Alloys and their Grain Refinement Potency in Aluminium Alloys, *Material Science Forum*, 2015, 828-829, p 23-28

19. O. Savas and R. Kayikci, A Taguchi optimisation for production of Al–B master alloys using boron oxide, *J. All. Comp*, 2013, 580, p 232–38

20. H. E. Calderón, R. G. I. Hidalgo, Z. H. Melgarejo and O. M. Suárez, Effect of AlB2–Mg interaction on the mechanical properties of Al-based composites, *Mater. Sci. Eng A*, 2010, 527, p 2258–64

21. G.I. Eskin and D.G. Eskin, *Ultrasonic Treatment of Light Alloy Melts*, 2nd ed. 2014, CRC Press, Boca Raton

22. O.V. Abramov, *Ultrasound in Liquid and Solid Metals*, 1994, CRC Press, Boca Raton, FL, pp. 43–77, p 273–406.

23. K. S. Suslick and G. J. Price, Applications of ultrasound to materials chemistry, *Annu. Rev. Mater. Sci.,* 1999, 29, p 295–326.

24. O. Kudryashova and S. Vorozhtsov, On the Mechanism of Ultrasound-Driven deagglomeration of Nanoparticle Agglomerates in Aluminum Melt, *J.Met*, 2016, 68(5), p 1307-11

25. A.V. Timoshkin. Integrated refining and modifying of silumins by method of high-speed jet melt processing (in Russian; Moscow, 2003)

26. F. Wang, D. G. Eskin, T. Connolley and J. Mi, Effect of ultrasonic melt treatment on the refinement of primary Al3Ti intermetallic in an Al–0.4Ti alloy, *J. Cry. Growth*, 2016, 435, p 24–30

27. O.N. Carlson, Al-B phase diagram, Bull, *Alloy Phase Diagrams*, 1990, 11 (6), p 560–66.

28. Y. Birol, Aluminothermic reduction of boron oxide for the manufacture of Al-B alloys, *Mater. Chem. Phys*, 2012, 136, p 963-66

29. F. Ficici, S. Koksal, R. Kayikci and O. Savas, Investigation of unlubricated sliding wear behaviour of in-situ AlB2/Al metal matrix composite, *Adv. Comp. Letters*, 2011, 20(4), p 109-16

30. M. Nowak, L. Bolzoni and N. H. Babu, Grain refinement of Al–Si alloys by Nb–B inoculation. Part I: Concept development and effect on binary alloys, *Mater. Des*., 2015, 66, p 366-75

31. S. M. Jigajinni, K. Venkateswarlu and S. A. Kori, Computer aided cooling curve analysis for Al-5Si and Al-11Si alloys, *Inter. J. Eng., Sci.Tech.,* 2011, 3(6), p 257-72

32. V. Gutiérrez., G. González and A. García, Thermal Analysis of Grain Refinement and Modification of an A356 Cast Alloy, *Chem. Mater. Res.,* 2014, 6(6), p 52-62

33. M. X. Zhang, P.M. Kelly, M.A. Easton and J.A. Taylor, Crystallographic study of grain refinement in aluminum alloys using the edge-to-edge matching model, *Acta Mater*., 2005, 53, p 1427–38

34. S. Nafisi and R. Ghomashchi, Boron-based refiners: Implications in conventional casting of Al–Si alloys, *Mater. Sci. Eng. A*, 2007, 452–453, p 445–53

35. T.E. Quested and A.L. Greer, The effect of the size distribution of inoculant particles on as-cast grain size in aluminium alloys. *Acta Mater.*, 2004, 52, p 3859–68

36. J. A. Dantzig and M. Rappaz, *Solidification*, 2009, CRC Press, Boca Raton

37. Y. Birol, Effect of silicon content in grain refining hypoeutectic Al–Si foundry alloys with boron and titanium additions, *Mater. Sci. Tech*., 2012, 28 (4), p 385-89

38. P.S. Mohanty and J.E. Gruzleski, Grain refinement mechanisms of hypoeutectic Al-Si alloys, *Acta Mater*., 1996, 44, p 3749–60.

39. P.A. Tondel and G. Halvorsen, Grain refinement of hypoertectic Al-Si Foundry alloys by addition of boron containing silicon metal, *Miner. Metals. Mater. Soc*., 1993, p 783-90.

40. L. Yuan, D. Chao and L. Y. Xiang, Grain refining mechanism of Al-3B master alloy on hypoeutectic Al-Si alloys, *Trans. Nonferrous Met. China*, 2011, 21, p 1435-40

41. G. Wang, M. S. Dargusch, M. Qian, D. G. Eskin and D. H. StJohn, The role of ultrasonic treatment in refining the as-cast grain structure during the solidification of an Al–2Cu alloy, *J. Crys. Growth.*, 2014, 8, p 119–24

Figures

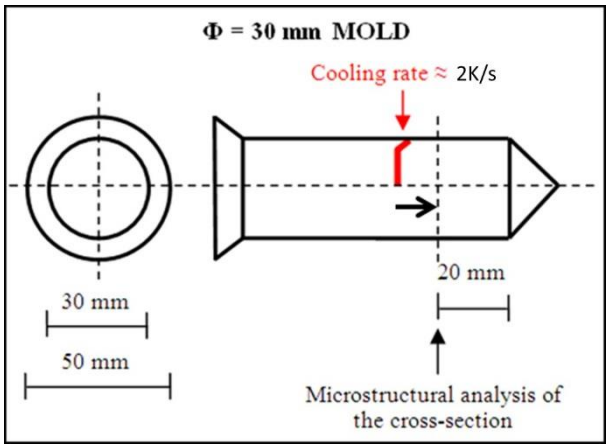

Figure 1. The schematic of metallic mould used for grain refinement studies

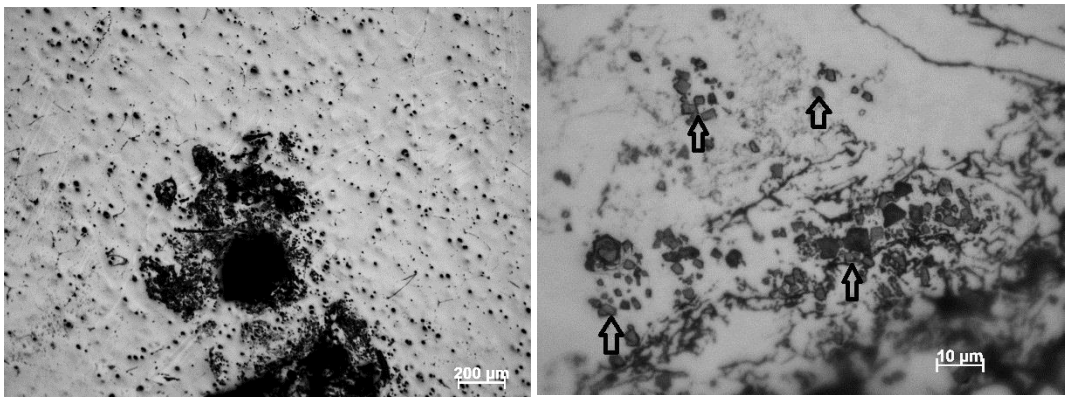

(a) (b)

Figure 2. Optical Micrographs of Al-B2O3 mix prepared by method 1 or 2 (a) large agglomeration present in the microstructure (b) reaction products observed near the agglomerate (shown by arrows)

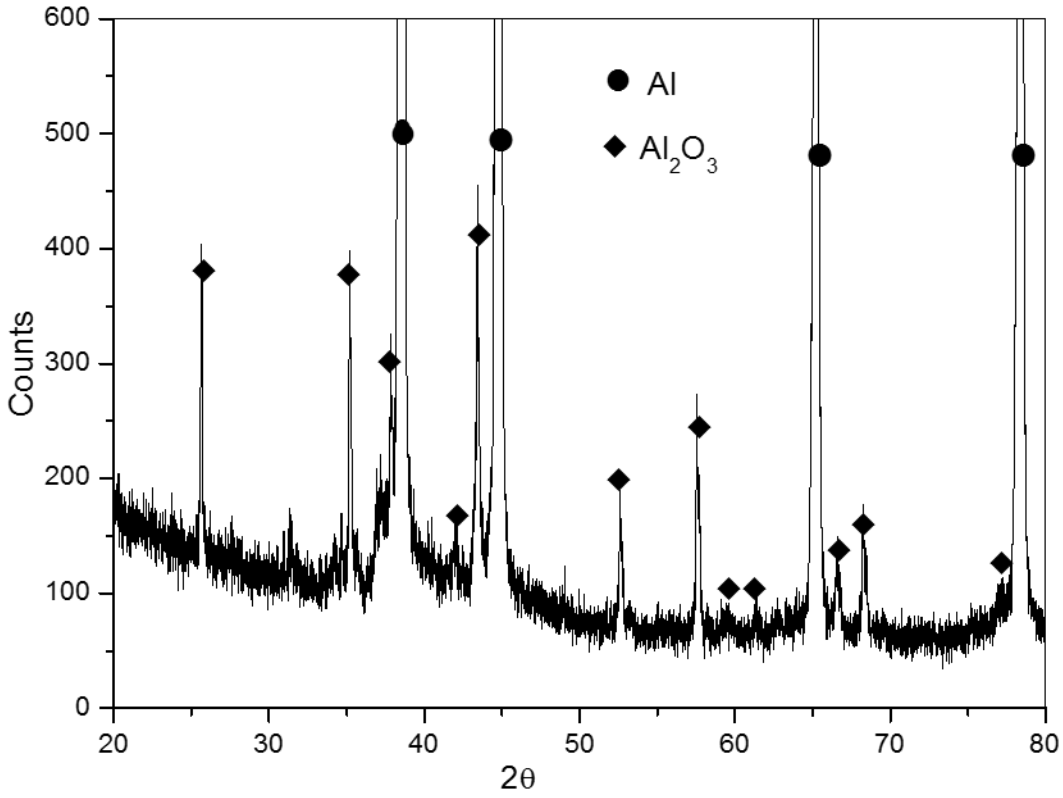

Figure 3. X-Ray Diffraction of Al-1.5B-7.6 Al_2O_3 master alloy

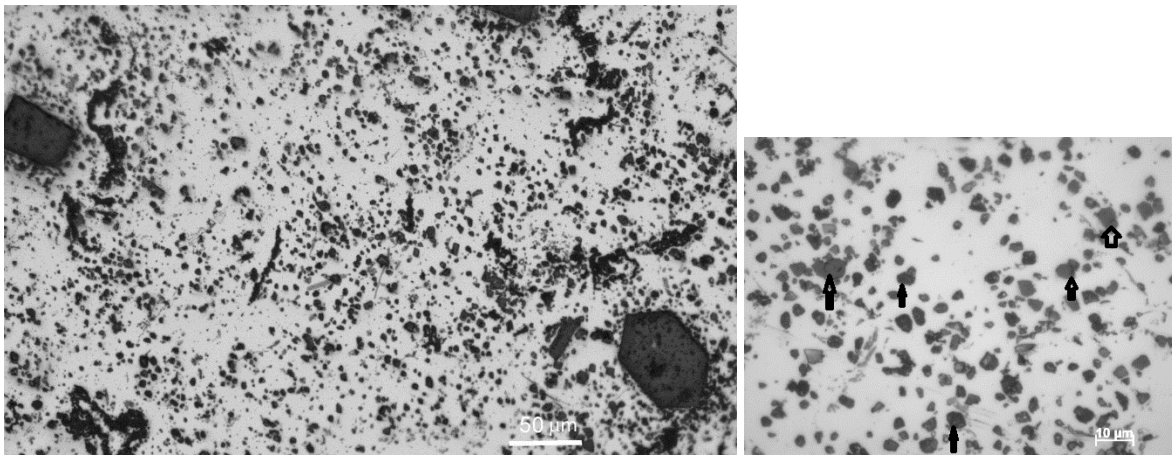

(a) (b)

Figure 4 (a&b). Optical micrographs of Al-1.5B-7.6Al_2O_3 prepared by method 3 (Al_2O_3 particles are represented by arrows in Fig 4b)

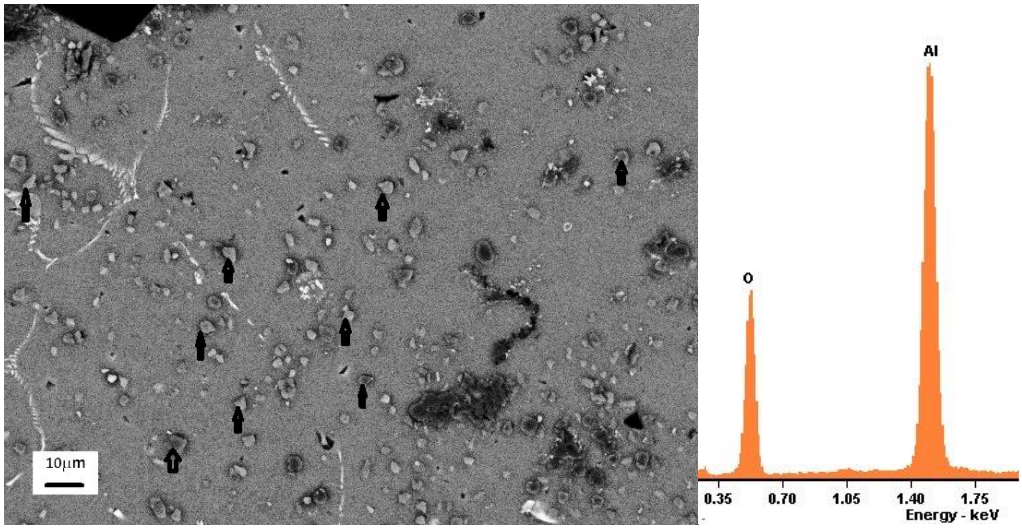

Figure 5. Al_2O_3 phases (shown by arrows) distribution in Backscattered SEM of Al-1.5B-7.6 Al_2O_3 prepared by method 3

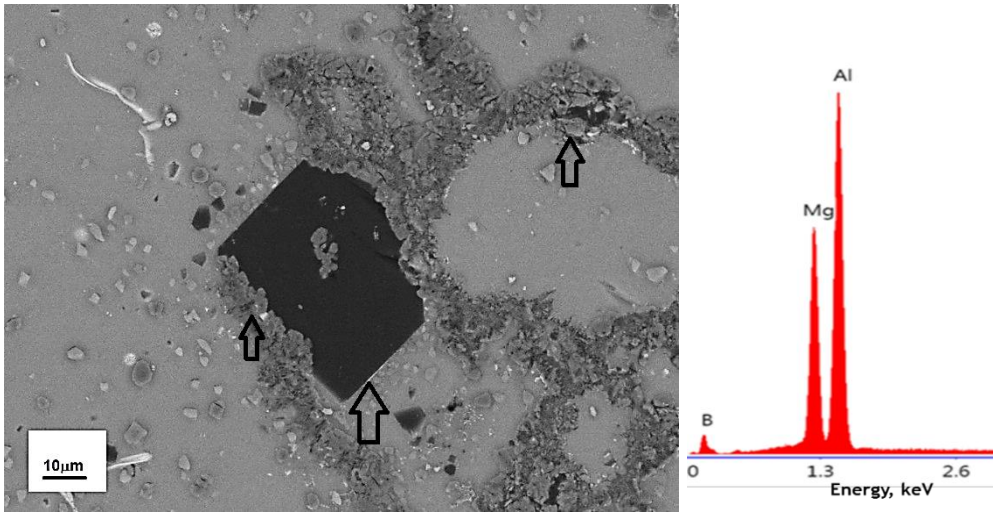

Figure 6. Al-Mg-B phase (dark blocky crystal shown by arrow) in Backscattered SEM of Al-1.5B-7.6 Al_2O_3 prepared by method 3

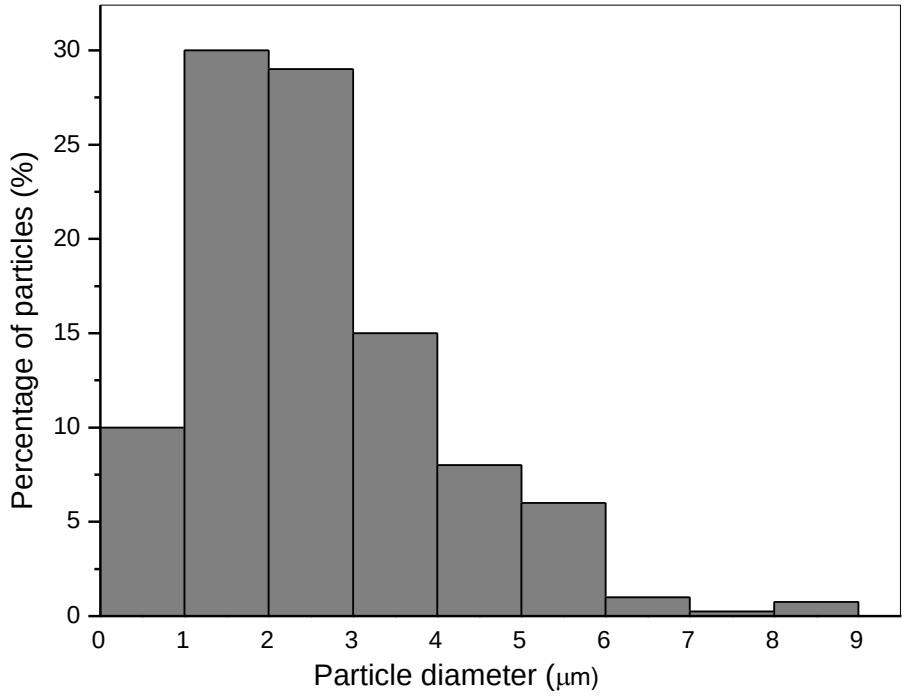

Figure 7. Al_2O_3 particle size distribution in Al-1.5B-7.6Al2O3 master alloy

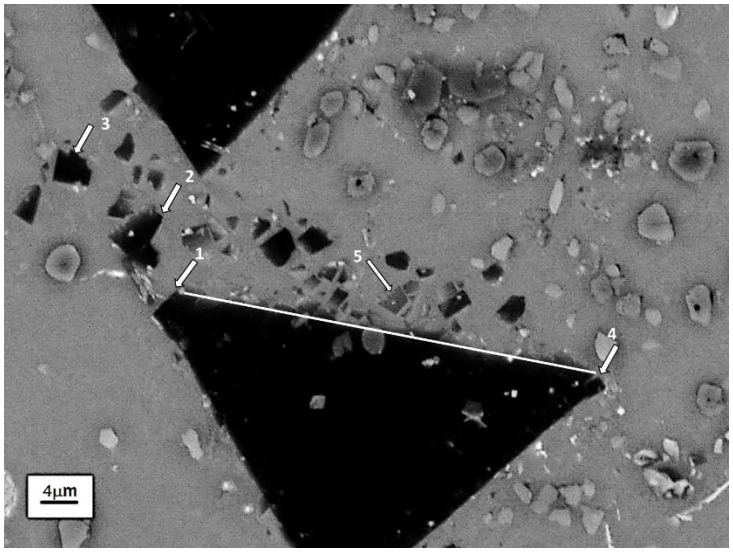

Figure 8. SEM micrograph of Al-1.5B-7.6 Al_2O_3 master alloy (possible mechanical disintegration of the crystal is shown from the micrograph)

(a) (b) (c) (d)

Figure 9. Macro etched CPAl (a) without master alloy addition and ultrasonication (b) with out master alloy addition and with ultrasonication (c) with master alloy addition and without ultrasonication (d) with master alloy addition and ultrasonication

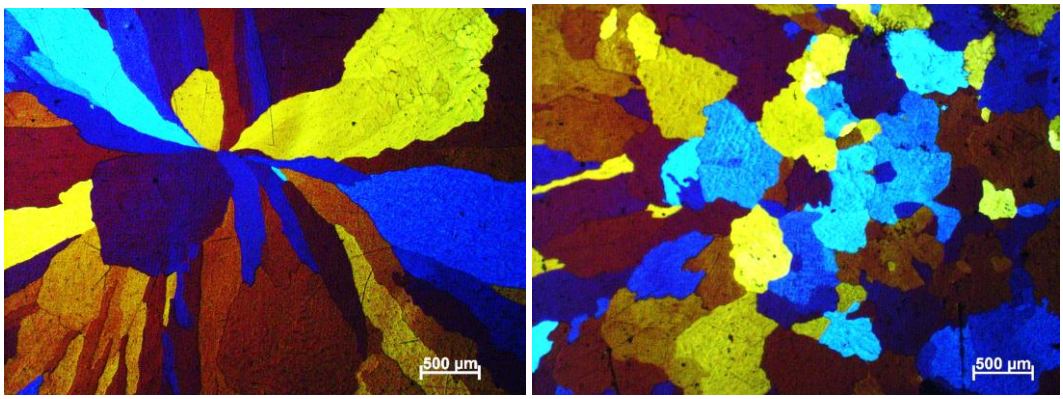

Figure 10. Anodized micrographs of CPAl cast (a) without master alloy addition and ultrasonication (b) with master alloy addition and ultrasonication

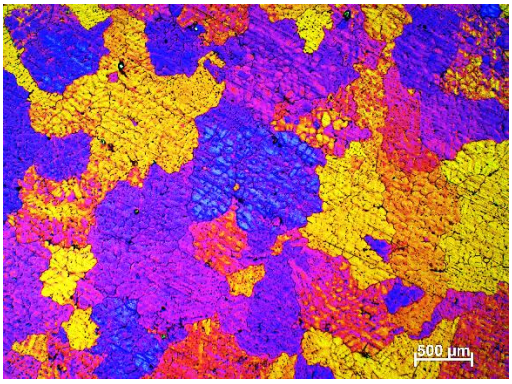

Figure 11. Anodized micrographs of Al-1.5Si-0.5Mg alloy cast without ultrasonication

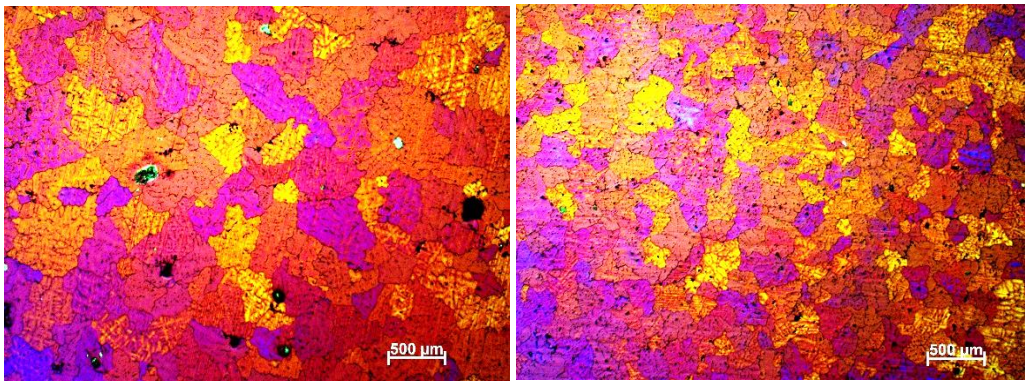

(a) (b)

Figure 12. Anodized micrographs of Al-1.5Si-0.5Mg+1wt% MA cast (a) without ultrasonication (b) with ultrasonication

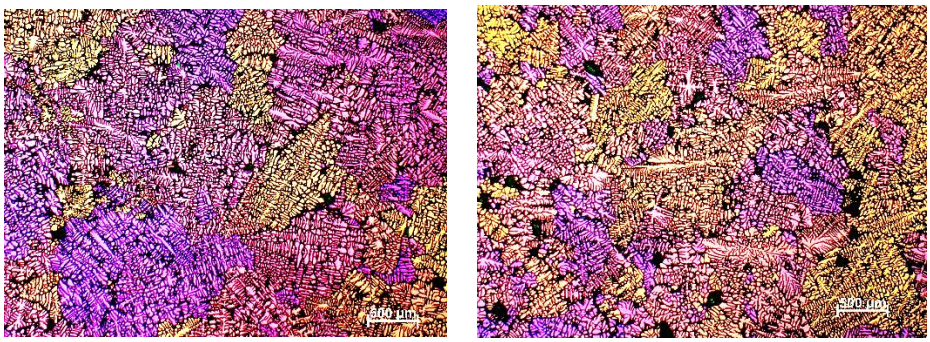

(a) (b)

Figure 13. Anodized micrographs of A357 cast (a) without ultrasonication (b) with ultrasonication

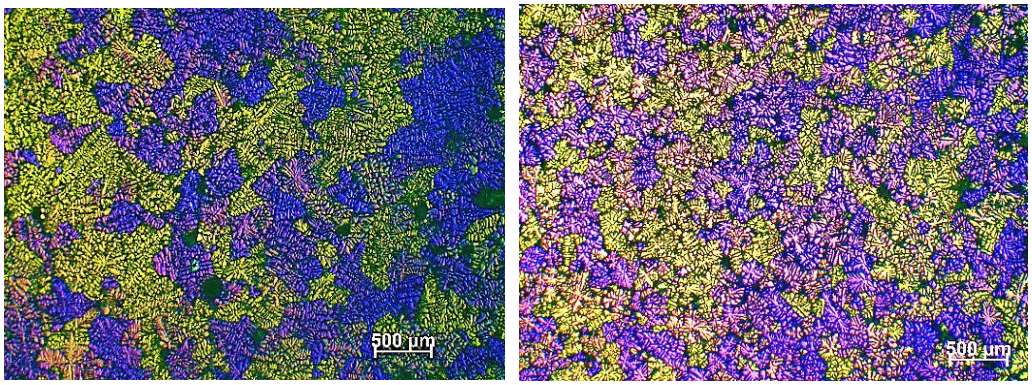

(a) (b)

Figure 14. Anodized micrographs of A357+1wt%MA and cast (a) without ultrasonication (b) with ultrasonication

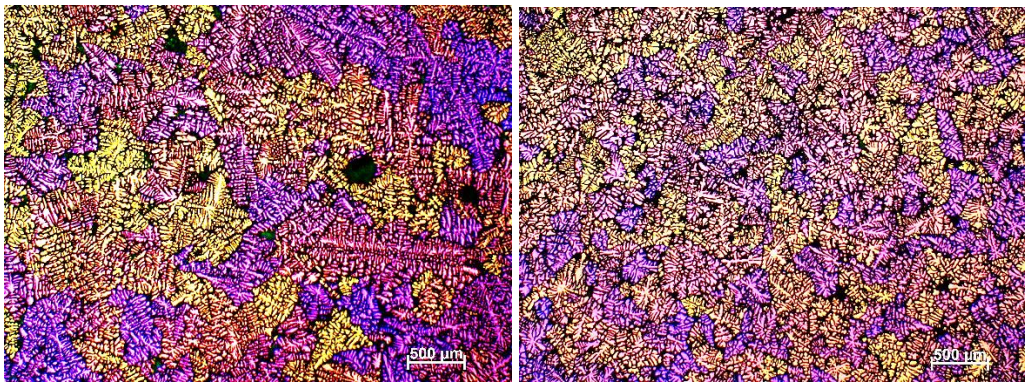

(a) (b)

Figure 15. Anodized micrographs of A357+0.1wt%MA and cast (a) without ultrasonication (b) with ultrasonication

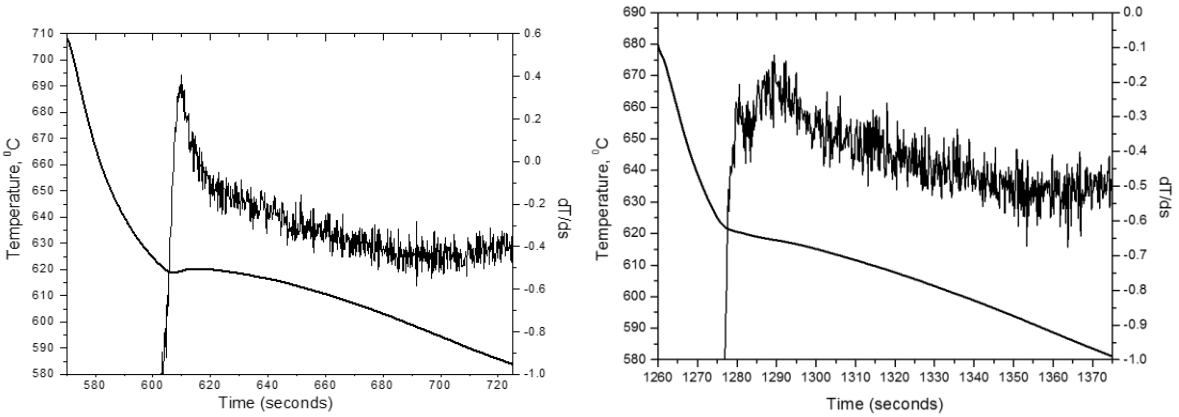

(a) (b)

Figure 16. Cooling curves of (a) A357 (b) A357 inoculated with 1wt% MA

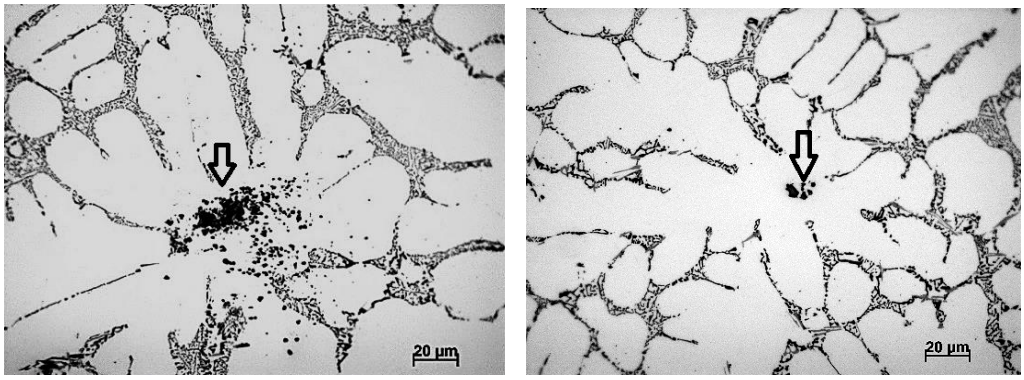

(a) (b)

Figure 17. Optical micrographs of A357+1wt%MA (a) without ultrasonication (b) with ultrasonication (particle clusters are shown by arrows)

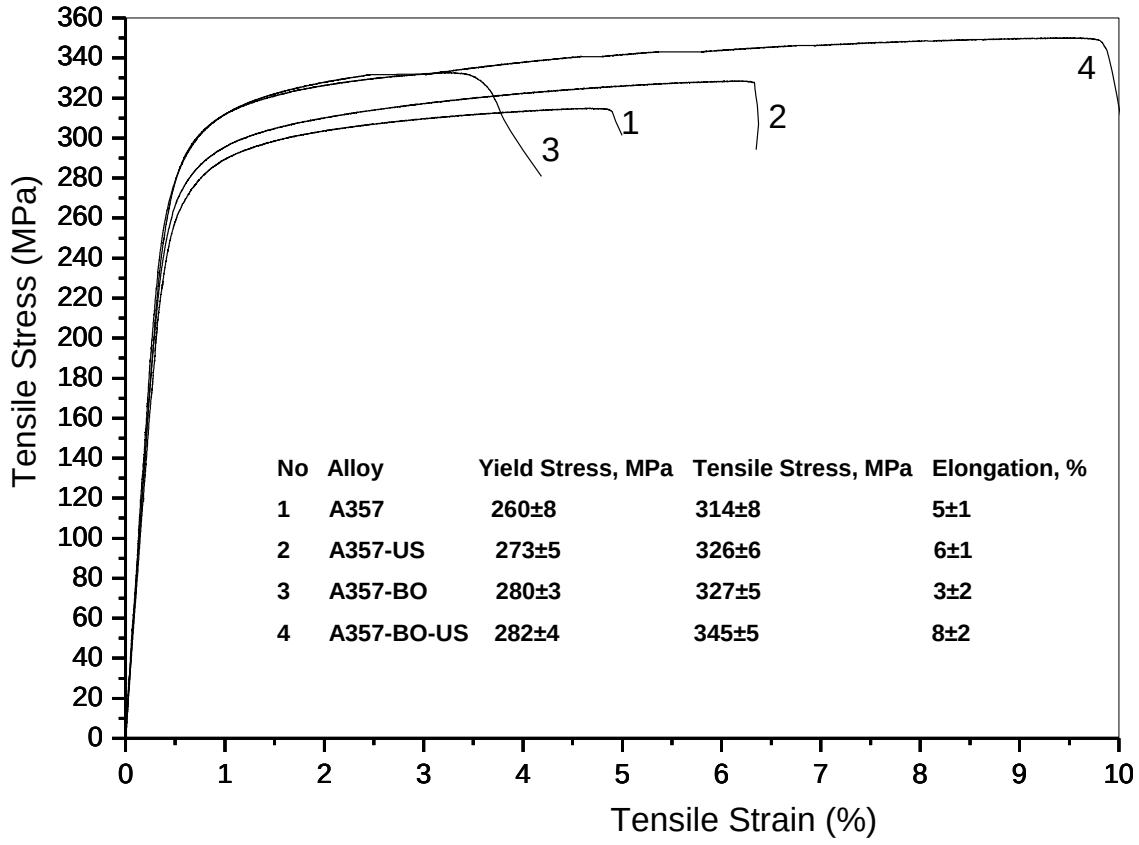

Figure 18. Tensile stress-Tensile strain curves of A357 alloys inoculated with Al-1.5B-7.6Al2O3 master alloy and treated with ultrasonication. The values are given in a table inside the figure